Encapsulation of InP/ZnS quantum dots into MOF-5 matrices for solid-state luminescence: *ship in the bottle* and *bottle around the ship* methodologies.

Alexis Tran[a], *Rodolphe Valleix*[a†], *François Réveret*[a], *Lawrence Frezet*[a], *Federico Cisnetti*[a]*, *Damien Boyer*[a]*

[a] Université Clermont Auvergne, Clermont Auvergne INP, CNRS, ICCF, F-63000 Clermont-Ferrand

ABSTRACT

The utilization of InP-based quantum dots (QDs) as alternative luminescent nanoparticles to cadmium-based QDs, known for their toxicity, is actively pursued. However, leveraging their luminescent attributes for solid-state applications presents challenges due to the sensitivity of InP QDs to oxidation and aggregation-caused quenching. Hence an appealing strategy is to protect and disperse InP QDs within hybrid materials. Metal-organic frameworks (MOFs) offer a promising solution as readily available crystalline porous materials. Among these, MOF-5, composed of $\{Zn_4O\}^{6+}$ nodes and terephthalate struts, can be synthesized under mild conditions (at room temperature and basic pH), making it compatible with InP QDs. In the present work, luminescent InP QDs are successfully incorporated within MOF-5 through two distinct methods. Firstly, employing the bottle around the ship (BAS) approach, wherein the MOF was synthesized around

the QDs. Secondly, utilizing the ship in the bottle (SIB) strategy, the QDs were embedded via capillarity into a specially engineered, more porous variant of MOF-5. Comparative analysis of the BAS and SIB approaches, evaluating factors such as operational simplicity, photoluminescence properties, and the resistance of the final materials to leaching are carried out. This comparative study provides insights into the efficacy of these strategies for the integration of InP QDs within MOF-5 for potential solid-state applications in materials chemistry.

Introduction

Quantum dots (QDs) are a well-known class of emerging materials which find applications in many forefront fields such as biological imaging,[1] lasers,[2] displays[3] and solid-state lighting.[4] These semi-conducting nanoparticles feature electron confinement that provides exceptional optical properties, such as high photoluminescent quantum yields (PLQY), size-dependent emission tuning, narrow emissions, and a wide absorption range.[5] The most used QDs contain cadmium, but their use is increasingly restricted due to toxicity concerns (*e.g.*, REACH regulations in Europe). Indium phosphide (InP) QDs are the most widely studied alternative.[6,7] However, the luminescence properties of InP QDs are far less effective than those of their cadmium-based counterparts in terms of PLQY, particularly under prolonged photonic stress.[8] Furthermore, their susceptibility to rapid oxidation in ambient air severely constrains their current applicability.[9,10] Additionally, as other quantum dots (QDs),[11] InP QDs experience the aggregation-caused quenching (ACQ) effect, restricting their utilization in solid-state applications. To stabilize and avoid aggregation of InP QDs, the use of a protective inorganic matrix or hybrid host such as metal organic frameworks (MOFs) seem an attractive strategy. MOFs are a family of compounds consisting of an ordered assembly of metal ions (or metallic clusters) and organic ligands (linkers),

resulting in the formation of a single-, two- or three-dimensional network.[12] MOFs are therefore considered to be large-porosity materials with high specific surface areas, ideal as host matrices for nanoparticle encapsulation. Their potential applications can span from gas storage to sensors and catalysis.[13–15] Several studies have already demonstrated the effectiveness of encapsulating QDs in MOF-type matrices for solid state dispersion or for enhanced protection against external stresses. Either in "onto" or "into" modes, MOF@QD materials find applications, as reviewed for energy, photocatalysis or light-harvesting system.[16–18] As far as luminescent materials are concerned, examples of MOF/QD composites remain scarce[17,19] and, to the best of our knowledge, none of them is reported with InP. However, on the one hand it has been possible to embed InP/ZnS in other matrices such as silica shells[20] or layered double hydroxides (LDHs),[21] and on the other hand luminescent MOFs with cadmium-based QDs are still actively considered.[22,23] Thus, encapsulating InP QDs could be of high interest as compared to the state of the art in luminescent MOFs.[24,25]

To achieve the encapsulation of InP/ZnS QDs, we selected MOF-5. This archetypical MOF,[26] composed of $\{Zn_4O\}^{6+}$ clusters and terephthalate linkers,[27,28] was chosen for its low cost and ease of synthesis, including by a well-known short (2.5 h) room-temperature protocol in basic conditions.[29] However, the pore size of MOF-5 (< 2 nm) does not allow direct encapsulation of QDs (3 - 10 nm).[30] We therefore need to find alternatives for integrating these nanoparticles into structures.

In the present study, we investigate the encapsulation of InP/ZnS quantum dots (QDs) employing two distinct methodologies: the "bottle around the ship" (BAS) and the "ship in the bottle" (SIB) approaches.[17,31] In the BAS method, we performed the synthesis of the metal-organic framework (MOF) around the quantum dots. This involves an initial ligand exchange process to disperse the

QDs within the solvent used for the MOF synthesis, namely *N*,*N*-dimethylformamide (DMF). We chose a room-temperature protocol,[29] considering its compatibility with delicate nanoparticles like InP also due to the mitigation of strong acidity commonly associated with traditional solvothermal procedures, achieved by employing triethylamine (Et_3N) as a mild organic base. Alternatively, in the SIB approach, we modified the original MOF-5 synthesis by introducing cetyltrimethylammonium bromide (CTAB). CTAB has been previously identified as a template agent for creating mesoporous MOF-5 structures under solvothermal conditions.[32] This modification enabled the incorporation of QDs into the MOF structure through capillarity.

These two distinct approaches allow us to explore and compare different strategies for the encapsulation of QDs within MOF frameworks, offering insights into their effectiveness and potential applications. For both strategies, electron microscopy, X-ray diffraction (XRD) and nitrogen physisorption were employed to characterize the obtained materials. The quantities of QDs incorporated into the different matrices were determined by UV-vis spectroscopy and ICP-OES. Finally, the solid-state luminescence properties of the newly prepared MOF@QD materials are presented.

Experimental Section

Synthesis of InP/ZnS QDs. The QDs synthesis and characterization was carried out following an established procedure.[21] $InCl_3$ (99.5 mg, 0.45 mmol, 1 eq.), $ZnCl_2$ (307 mg, 2.25 mmol, 5 eq.) and oleylamine (5 mL) were added to a 50 mL three-necked round-bottomed flask in an argon-filled glovebox. The flask was equipped with a reflux condenser and connected to a Schlenk line. A temperature probe was inserted through one of the necks and the last one was equipped with a septum to allow the addition of reagents. The mixture was heated at 120°C under vacuum

(0.20 mbar) to dissolve metal salts and remove oxygen as well as water traces. The flask was then filled with argon and the temperature was set to 180°C before the injection of tris-(diethylamino)phosphine ($P(DEA)_3$) (0.49 mL, 1.80 mmol, 4 eq.). For the ZnS shell deposition, tri(*n*-octyl)phosphine sulfide (TOP-S) was separately prepared by stirring precursors (tri(*n*-octyl)phosphine: 10 mL, 8.3 g, 22.4 mmol; and elemental sulfur: 0.718 g, 22.4 mmol) for 1h at 100°C under argon atmosphere. The crude mixture containing QDs was maintained at 180°C and 0.4 mL TOP-S was added dropwise to the InP core. The mixture was allowed to react for 2 hours. Then the zinc precursor solution was added (1.5 g of zinc stearate in 6 mL of octadecene and 2 mL of oleylamine) and the temperature set to 260°C. Once the temperature reached 200°C, 1.4 mL of TOP-S was added dropwise over 10 minutes. The mixture reacted at 260°C for 1.7 hours. The mixture was cooled to room temperature. The mixture was purified with 3 cycles of precipitation/redispersion with an absolute ethanol/chloroform mixture (1/4 – v/v) and the precipitate was recovered by centrifugation (11000 rpm/15 min). After these purification steps, the QDs were suspended in chloroform and stored in a fridge with a concentration of about 60 $g.L^{-1}$. These suspensions remain stable for months. Structural and optical characterizations are described in the Supporting Information (**Figure S1** and **S2**).

Ligand exchange of OLAm-capped InP/ZnS with 6-mercaptohexan-1-ol (MCH). The ligand exchange of oleylamine-capped InP/ZnS QDs was performed following a modification of an existing method.[33] The as-synthesized suspension (0.9 mL, 54 mg of QDs for a suspension of 60 $g.L^{-1}$) was placed in a three-necked round bottom flask under argon. A solution of a large excess of MCH (2 mL, 11 mmol) in 5 mL of DMF was added to the suspension of QDs. The mixture was heated to 120°C with stirring (1000 rpm) and left to react for 30 min. During this time, the QDs and DMF formed an apparently homogeneous suspension. The mixture was cooled to room

temperature. The QDs were purified by two cycles of precipitation/redispersion by using centrifugation (11 000 rpm, 15 min) with a 25 mL mixture of isopropanol/toluene (1/5 – v/v). The resulting solid (0.6 g) was then suspended in an adjusted volume of DMF to obtain a 60 g. L^{-1} suspension of QDs before being stored in a fridge. Suspensions remain stable for several months. Structural and optical characterizations are described in **Figures S3** and **S4**.

Synthesis of MOF-5 and MOF@QD. The MOF-5 material was synthesized at room temperature using a protocol described by Tranchemontagne *et al.*[29] Terephthalic acid (0.085g, 0.5 mmol, 1 eq.) and triethylamine (0.135 mL, 1 mmol, 2 eq.) were dissolved in 5 mL of DMF. Separately, zinc acetate dihydrate (0.285 g, 1.3 mmol, 2.6 eq.) was dissolved in 5 mL of DMF. The zinc salt solution was added to the organic solution, which was magnetically stirred at 700 rpm for 2.5 h. The precipitate was collected by centrifugation (10000 rpm, 15 min). Then, it was subjected to washings with 1 x 15 mL of DMF to remove the excess of zinc salt, and 2 x 15 mL chloroform to remove the residual organic ligands while recovering each time the solid by centrifugation (same conditions as above). The powder was dried at 60°C overnight before characterization. For the preparation of MOF@QD samples, the same MOF-5 synthesis was performed, but in each reaction mixture, a certain volume of the 60 $g.L^{-1}$ DMF suspension of MCH-InP/ZnS QDs was added (0.1 to 0.3 mL corresponding to 6 to 18 mg of QDs). Other volumes were adjusted to keep the total volume at 10 mL. The material purification method was the same as for pristine MOF-5.

Synthesis of mesoporous MOF-5/CTAB. Mesoporous MOF-5 was prepared using CTAB as template agent. For the same conditions and the same quantities of reagents as described above for the synthesis of MOF-5 at room temperature, CTAB (ranging from 18 mg to 54 mg, corresponding to 0.1 - 0.3 eq.) was dissolved with terephthalic acid and triethylamine. The MOF-5/CTAB hybrids were worked up in the same manner as described above.

Preparation of MOF@QD/x CTAB samples. Hybrid materials were prepared by using 0.1 g of MOF-5/x CTAB. 0.3 mL of a suspension of InP/ZnS QDs (60 $g.L^{-1}$ in chloroform, 18 mg) and 5 mL of chloroform were added to the MOF-5/CTAB powder. The vial was heated at 60°C using a hot sand bath until total evaporation of the solvent. The final material was suspended in chloroform and then washed 3 × with 10 mL of chloroform. The precipitate was collected by centrifugation (11 000 rpm/10 min) between the different washes. The final material was then dried 60°C overnight before analysis.

Characterizations.

X-ray diffraction experiments were performed with a X'Pert Pro diffractometer with a Cu-Kα radiation (λ = 0.15418 nm) over 2θ angles ranges from 5 to 50°. **Scanning electron microscopy** was performed on Jeol 6060-low vacuum apparatus. The samples were prepared by deposition on a carbon tape and gold sputtering metallization. **Nitrogen physisorption** was performed on a Micromeritics 3-Flex in the Chemical institute of Rennes (France). The different samples were degassed at 200°C for 24 h before analysis. All calculations: Brunauer, Emmet and Teller (BET) and Barret, Joyner and Halenda (BJH) are performed using Flex software developed by micromeritics **Photoluminescence quantum yield** measurements (PLQY) and fluorescence spectra (including EEM) were recorded with an integrating sphere measurement system from Hamamatsu photonics (C9920-02G). The system is composed of a 150 W Xenon lamp, and integrating sphere coated with Spectralon and a CCD camera for the detection. The internal photoluminescence quantum yield $PLQY_{int}$ and the absorption coefficient (Abs) defined by formulae 1 and 2 were obtained directly from the measurements made in the integrating sphere. The external photoluminescence quantum yield $PLQY_{ext}$ was calculated from the product of

$PLQY_{int}$ and Abs, and corresponds to the number of emitted photons over the number of incident photons (formula (3)).

(1) $PLQY_{int}$ = n. emitted photons/n. absorbed photons

(2) Abs = n. absorbed photons/n. incident photons

(3) $PLQY_{ext} = PLQY_{int} \times Abs$ = n. emitted photons/n. incident photons.

Semi-quantitative **emission spectra** were recorded using a 375 nm picosecond laser diode (75 ps and 20 MHz for the pulse duration and the repetition rate) combined with a 300 mm focal length monochromator (FLS 980) and a photomultiplier Hamamatsu R928P. **UV assays** and **fluorescence spectra in solution** were performed with a Duetta Fluorescence and Absorbance spectrometer. **ICP-OES** analyses for Indium were conducted using an ICP-OES 5800 Agilent (USA) in an axial mode at 230.606 nm. The solid sample were first mineralized. 50.0 mg of powder were introduced into a hermetically sealed Teflon microwave reactor (MW5000 Anton Parr) with 2 mL HCl (37 %) and 6 mL HNO_3 (68 %). The reactors were placed in an Anton-Paar microwave oven and heated (10°C/min ramp) to 230°C for 30 min. The acidic solutions were then recovered and diluted in a 50 mL volumetric flask with deionized water prior to ICP analysis. **Scanning transmission electron microscopy coupled with a high-angle annular dark-field detector (STEM-HAADF)** was performed on QDs in suspension in $CHCl_3$ using a FEI Titan Themis microscope operating at 200kV; QDs were dropped on a Lacey Carbon membrane. QDs were dried at room temperature before introducing them into the microscope.

Results and discussion

InP/ZnS QDs were synthesized following modified procedure.[21] They exhibit a bright red emission signal centered at 625 nm **(Figure 1** and **Figure S2)**, they present a photoluminescence quantum yield (PLQY) in solution of 50 %. However, these nanoparticles experiment aggregation-caused

quenching (ACQ) and exhibit a solid $PLQY_{ext}$ at 370 nm of 5.6 % (**Figure S2b**). Then, in order to improve their compatibility with the synthesis medium of the MOF, we intended to perform a surface ligand replacement. In order to do this, the native oleylamine was replaced with 6-mercaptohexan-1ol (MCH). After several washing steps, the QDs were DMF-dispersible, thus compatible with a MOF synthesis. We will later refer to the QDs obtained through this procedure as MCH-QDs (or MCH-InP/ZnS). Only slight changes are noticed after the ligand exchange. A slight red-shift of both the absorption and emission of the QDs, but the width of the emission remains constant (**Figure 1**).

The *bottle around the ship* (BAS) approach

MOF-5 matrices have been synthesized in presence of MCH-InP/ZnS QDs. Over the course of the synthesis, no change in the color of the solution was noticed. Additionally, upon UV light excitation (λ_{exc} = 365 nm) no alteration was visible in the luminescence of the solution. At the end of the synthesis and after several washing steps, the obtained material remained red, highlighting the presence of the QDs into the MOF-5 structure (**Figure S5**). To quantify the amount of QDs incorporated in the hybrid materials, we performed a spectrophotometric analysis of MCH-InP/ZnS QDs still present in suspension in DMF after the MOF-5 synthesis. Briefly, the quantity of integrated $(InP)_i$ is determined by calculating the difference between the quantity of MCH-QDs employed in the synthesis and the quantity of MCH-QDs still detected in the supernatant. The quantity of $(InP)_i$ is calculated using the equations given in the Supporting Information from the absorbance at 413 nm.

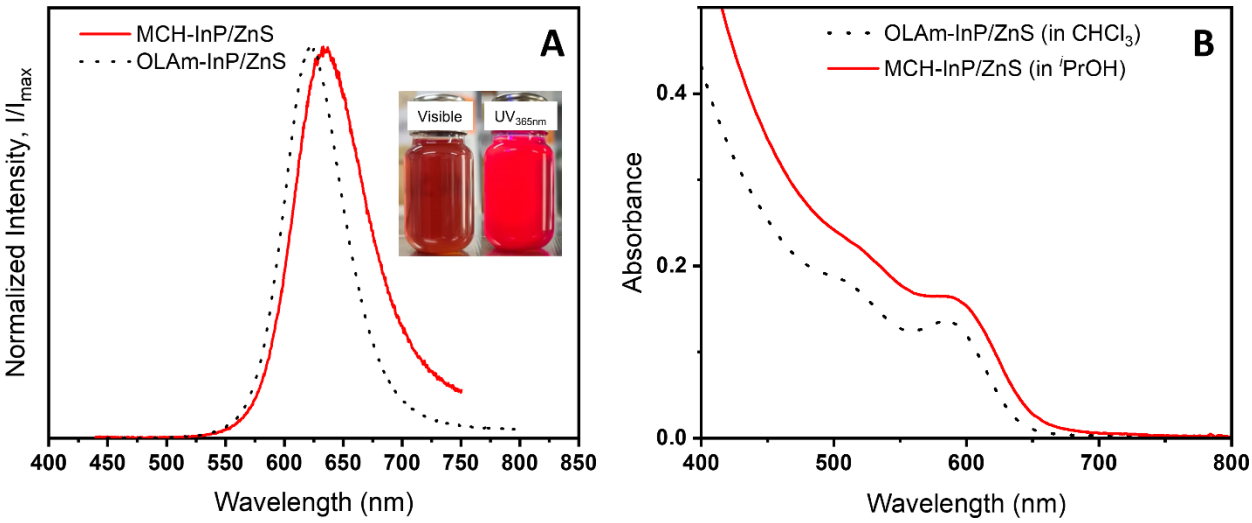

Figure 1. (A) Emission and (B) absorption spectra of InP/ZnS QDs before (dotted line) and after (red) ligand exchange with 6-mercaptohexan-1-ol. Inset in (A): photographs of MCH-InP/ZnS under visible and UV (λ_{exc} = 365 nm).

Table 1. $(InP)_i$ integration percentages in the various MOF@QD samples.

QDs mass	$A_{413\ nm}$	Initial amount of $(InP)_i$ (mmol)	Amount of residual $(InP)_i$ (mmol)	Amount of integrated $(InP)_i$ (mmol)	% integration
6 mg	0.12	4.0×10^{-2}	1.2×10^{-2}	2.8×10^{-2}	70
12 mg	0.21	8.0×10^{-2}	2.16×10^{-2}	2.16×10^{-2}	73
18 mg	0.34	1.2×10^{-1}	4.2×10^{-2}	7.8×10^{-2}	65

In all syntheses, the majority of QDs is incorporated into the structure (**Table 1**), with values close to 70 % for all the samples. By considering the mass obtained for the different samples after synthesis, it is possible to give a value for incorporated InP in mmol per gram of material. These values can be confirmed by ICP-OES (**Table 2**).

Table 2. Determination of the amount of $(InP)_i$ in mmol/g of final material synthesized and designation for every MOF@QD_x sample prepared.

QDs mass	Mass recovered (g)	mmol of $(InP)_i$/g of final material (UV-Vis)	mmol of $(InP)_i$/g of final material (ICP-OES)	Sample designation
6 mg	0.101	0.28	0.30	MOF@$QD_{0.3}$
12 mg	0.107	0.55	0.62	MOF@$QD_{0.6}$
18 mg	0.113	0.69	0.75	MOF@$QD_{0.7}$

Then, we studied the impact of the amount of QDs on the structural and morphological properties of the samples. Despite the presence of InP/ZnS QDs in the sample, the powder XRD patterns of the synthesized samples are similar to those reported in the literature. The presence of QDs in MOF-5 matrices cannot be highlighted with this technique because the concentration of QDs incorporated is too low. The (200), (220), (400) and (420) main diffraction peaks of MOF-5 (**Figure 2A**) are respectively present at $2\theta = 6.8°, 9.7°, 13.7°$ and $15.4°$ suggesting a microcrystalline powder.[27] We noticed for the MOF@$QD_{0.7}$ an inversion of the intensity ratio between the diffraction peak at $2\theta = 6.8°$ and $9.7°$ which may arise from the presence of lattice interpenetration and zinc-based species within the MOF pores.[34]

To identify the presence of particles in the pores of MOF-5, we measured the specific surface area by nitrogen physisorption after the insertion of QDs in the structure. The various isotherms are of type I according to the IUPAC classification, evidencing the microporous nature of the various samples analyzed. By comparing the isotherms of MOF@QD_x with a classic MOF-5 synthesized in same conditions, we observed a decrease of the specific area with increasing QDs loading rate (**Figure 2B**).

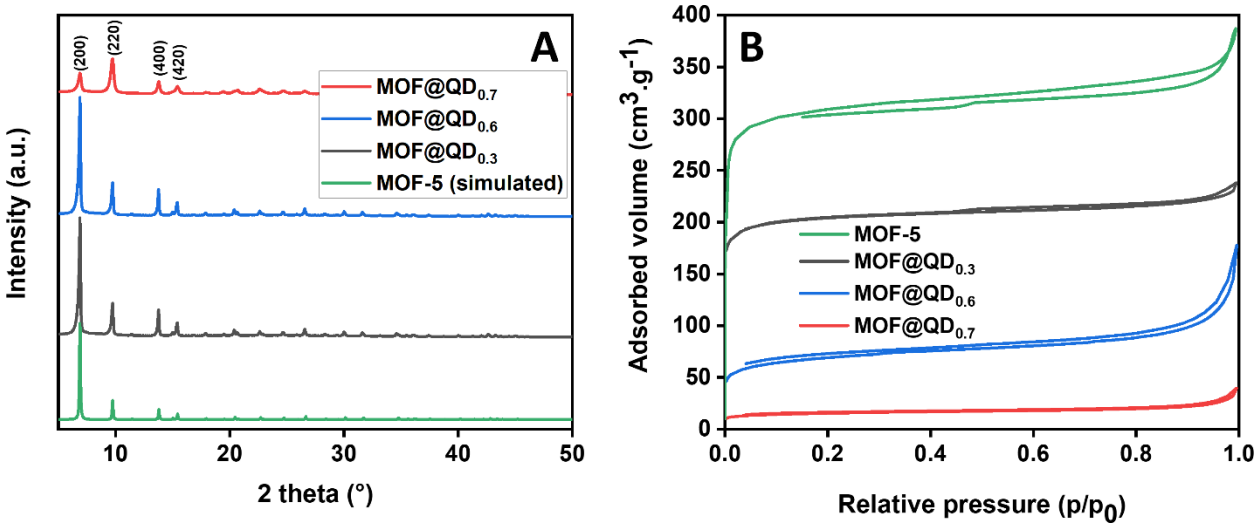

Figure 2. (A) Powder XRD pattern and (B) Adsorption and desorption isotherms of MOF-5[26] and synthesized MOF@QD_x (x = 0.3, 0.6, 0.7).

Logically, as the loading of QDs increases, the specific surface area of the various samples decreases, resulting from the increasing congestion of the porosity. In addition to the fact that the luminescence of MOF@QD_x is conserved after several washings, these measurements seem consistent with the encapsulation of QDs within the MOF-5 matrix (**Table 3**).

Table 3. BET and BJH results for different MOF@QD_x samples synthesized by the BAS method.

Sample	S_{BET} ($m^2.g^{-1}$)	Pore size (BJH) (nm)
MOF-5	940	4.5
MOF@$QD_{0.3}$	655	4.4
MOF@$QD_{0.6}$	234	4.3
MOF@$QD_{0.7}$	51	4.8

The near-complete disappearance of the initial specific surface area of MOF-5 in the sample prepared with the highest initial quantity of QDs strongly indicates that this loading approaches its

maximum capacity. Interestingly, our observations reveal that despite the increased QDs quantity during synthesis, the pore size (calculated using the BJH method) remain constant and consistently smaller than the size of QDs. This finding suggests that if the QDs are encapsulated, it does not occur through direct insertion into the pre-existing MOF porosity; it rather happens through the formation of the matrix around the QDs during the synthesis process.

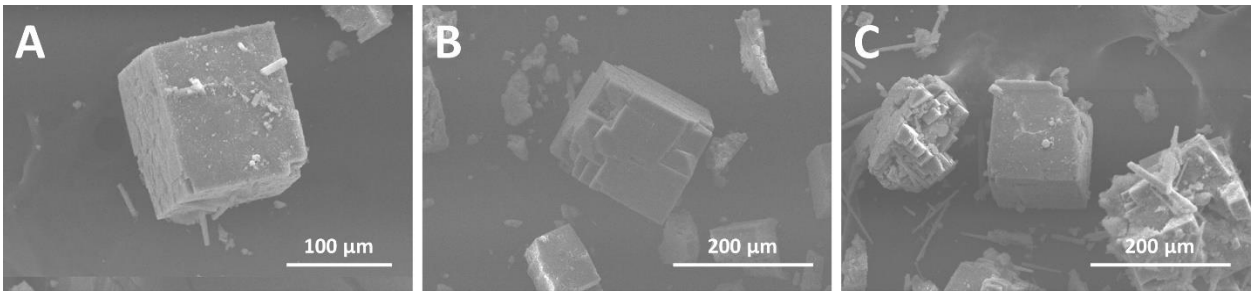

Figure 3. SEM images of (A) MOF@$QD_{0.3}$, (B) MOF@$QD_{0.6}$, and (C) MOF@$QD_{0.7}$.

SEM images reveal the presence of cubic crystals, with and average size of 100-150 µm, corresponding to the microscopic organization expected for MOF-5 (**Figure 3**). However, the greater the initial quantity of QDs in the synthesis, the more the structure exhibits apparent defects. Cracks and even different microstructures were observed, particularly in the MOF@$QD_{0.7}$ sample: the QDs create large defects in the structure, causing irregularities in the crystal appearance.

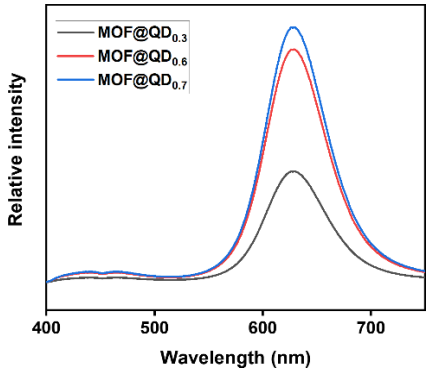

Figure 4. Emission spectra of MOF@QD_x synthesized by the BAS approach (λ_{exc} = 375 nm).

The optical properties of the above obtained materials were then investigated (**Figure 4**). The maximum emission wavelength of those samples is at 628 nm (a slight hypsochromic shift compared with 634 nm for QDs after ligand exchange). The two samples with the highest QDs loading (for x = 0.55 and 0.69) present emission intensities that are close. However, they display twice the emission intensity of the MOF@$QD_{0.3}$. The emission of the samples tends towards a maximum intensity as a function of the loading ratio. Doubling the amount of QDs in solution during the integration step does not double the maximum emission intensity. In MOF@$QD_{0.7}$, reabsorption or aggregation phenomena (several QDs stacked within a pore) may occur, which could explain the lower intensity.

Table 4. PLQY measured for λ_{exc} = 365 nm on the different MOF@QD_x prepared by the "BAS" method.

Sample	$PLQY_{int,\ 365nm}$ (%)	Absorption Coefficient	$PLQY_{ext,\ 365nm}$ (%)
MOF@$QD_{0.3}$	13	0.32	4.2
MOF@$QD_{0.6}$	10	0.61	6.1
MOF@$QD_{0.7}$	8	0.90	7.2

The PLQY of the different samples are compared (**Table 4**) to verify the hypotheses set out above. The $PLQY_{int}$ decreases with increasing QDs loading, while the absorption coefficient increases. However, the slight drop in $PLQY_{int}$ is offset by the increase in absorption coefficient, so that the sample with the best $PLQY_{ext}$ is MOF@$QD_{0.7}$ (consistent with the spectra, **Figure S6**).

Leaching tests were performed on these samples, leaving the powders in chloroform for several hours. No decrease in intensity was observed over time, showing once again that the particles are well confined inside the MOF (**Figure S7**).

The *ship in the bottle* (SIB) approach

For the SIB approach, as the porosity of MOF-5 does not allow the direct encapsulation of QDs by capillarity – the average pore size being only 4 nm – we sought to prepare mesoporous MOF-5. For the sake of simplicity, we first decided to check whether the modification of the solvothermal preparation of MOF-5 by addition of CTAB was also transposable to our experimental conditions (*i.e.*, room temperature and use of Et_3N[29]). The samples are designated as MOF-5/x CTAB, x being the molar ratio of CTAB used during the synthesis.

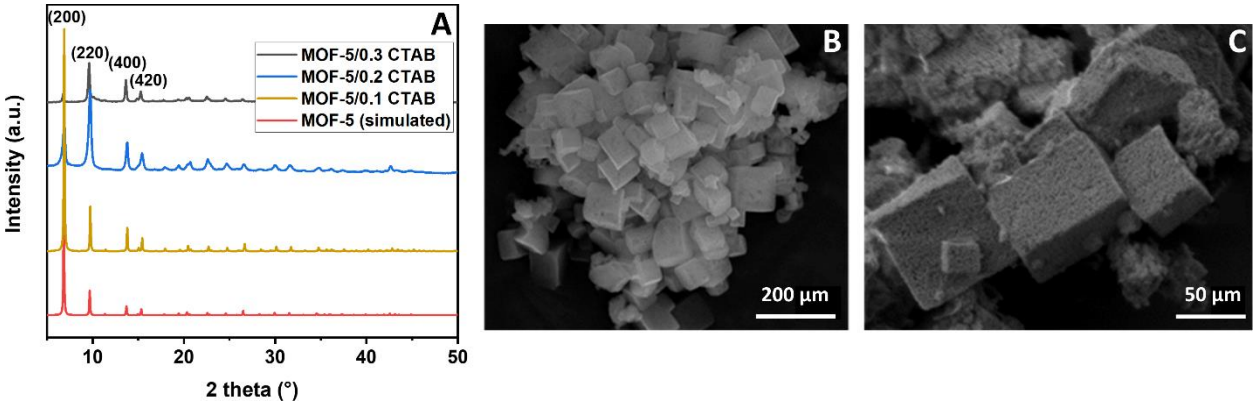

Figure 5. (A) Powder XRD patterns of simulated MOF-5[26] and synthesized MOF-5/x CTAB (x = 0.1, 0.2, 0.3). SEM images of (B) MOF-5 and (C) MOF5/0.3 CTAB sample.

The XRD patterns recorded from MOF-5/x CTAB samples (**Figure 5A**) show diffraction peaks corresponding to the (200), (220) (400) and (420) reticular planes at $2\theta = 6.8°$, 9.7°, 13.7° and 15.4°, respectively. While the sample synthesized with the least amount of CTAB exhibits a

diffractogram similar to the simulated one. As the quantity of CTAB in the synthesis increases, the relative intensities of diffraction peaks of the (200) and (220) become inverted but no explanation can be given for this observation. However, despite this difference, the diffractograms still correspond to the expected structure for the MOF-5.

SEM image (**Figure 5C**) recorded from the MOF-5/0.3 CTAB displays a cubic morphology typical for MOF-5. However, the presence of CTAB in the synthesis seems to induce the formation of a new porosity. Indeed, asperities on the surface are undoubtedly visible on the images. This is in strong contrast with the smooth surface obtained in the case of unmodified MOF-5 (**Figure 5B**). Since the pore size is not accessible by direct SEM observation, MOF-5/x CTAB materials were analyzed by nitrogen physisorption to determine the new specific areas and porosities.

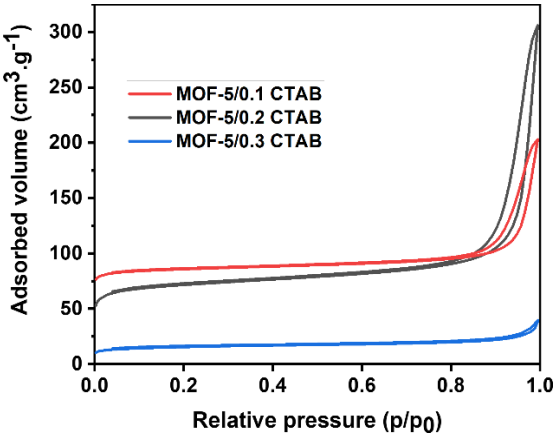

Figure 6. Adsorption and desorption isotherms of MOF-5/x CTAB (x = 0.1, 0.2, 0.3).

According to IUPAC classification, the isotherms correspond to type I. The higher the amount of CTAB in the synthesis, the lower the specific surface area of the MOF. This means that either the porosity becomes clogged, or the pore size increases, thus reducing the level of microporosity within the structure. The drop-off at desorption level indicated the presence of mesoporosity.

Table 5. BET and BJH analyses on MOF-5/x CTAB samples.

Sample	S_{BET} ($m^2.g^{-1}$)	Pore size (BJH) (nm)
MOF-5/0.1 CTAB	329	20
MOF-5/0.2 CTAB	233	21
MOF-5/0.3 CTAB	50	48

The specific surface areas measured are all much lower than the 940 $m^2.g^{-1}$ obtained with the MOF-5 (**Table 3**). Increasing the CTAB content decreases the specific surface areas of the MOF-5 and increases the pore opening values that are all larger than the size of the QDs (from 20 to 48 nm *vs.* 3 – 10 for typical QDs). These pore sizes are consistent with those reported by Ren *et al.* in solvothermal conditions.[32] The modification of the MOF-5 synthesis involving the addition of CTAB allowed to considerably increase pore size for direct encapsulation of nanoparticles without altering the structural properties of MOF-5.

In each of these synthesized mesoporous matrices, 18 mg of MCH-InP/ZnS QDs are incorporated per 100 mg of MOF-5, which is the amount used previously for the BAS technique. After inserting QDs into matrices, samples are designated as MOF@QDs/x CTAB with x the molar ratio of CTAB used during the MOF-5 synthesis. The final powder obtained after insertion of QDs by this SIB protocol has a much more intense red color than that prepared by the BAS approach. Under UV excitation (λ_{exc} = 365 nm), the luminescence of these powders results in a strong red emission (**Figure S8**). Washing steps did not apparently diminish the luminescence of the final hybrid material, showing that the QDs were not simply deposited on the MOF surface but were well-incorporated within the structure. In stark contrast, the attempted insertion of QDs into MOF-5 prepared without CTAB failed as no red color nor luminescence was observable after the various

washing steps. These initial indications underline the importance of CTAB in the preparation of MOFs, enabling larger porosity sizes to be obtained for the incorporation of InP/ZnS QDs.

Table 6. Determination of the amount of $(InP)_i$ in mmol/g of final material synthesized by ICP-OES.

Sample	mmol of $(InP)_i$/g of final material (ICP-OES)
MOF@QDs/0.1 CTAB	1.14
MOF@QDs/0.2 CTAB	1.11
MOF@QDs/0.3CTAB	1.12

The different remaining solutions after the washing steps showed no luminescence. The amount of QDs incorporated was therefore the same for each sample and equal to the initial amount of QDs used. The amount of QDs embedded has been confirmed by ICP-OES measurements (**Table 6**).

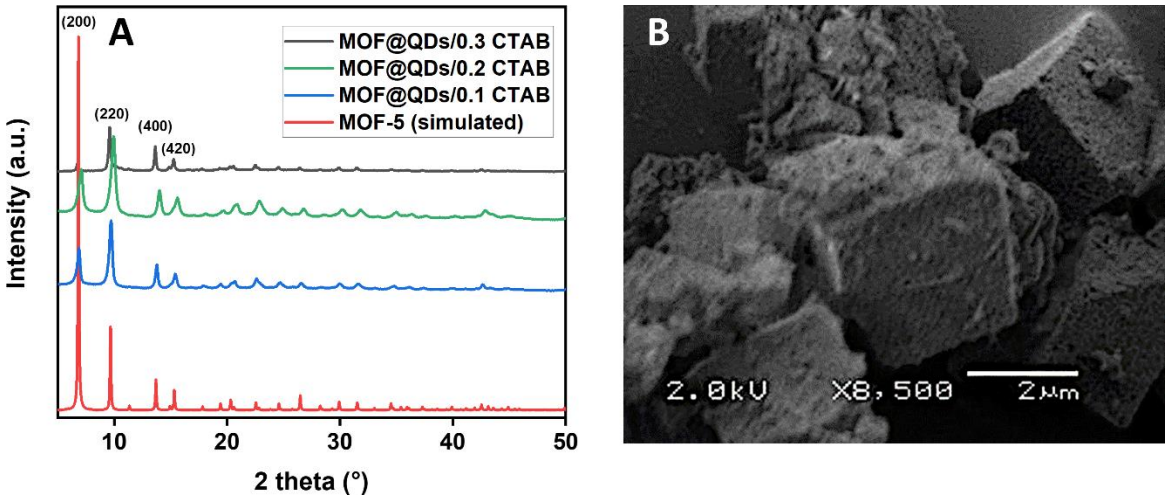

Figure 7. (A) Powder XRD patterns of simulated MOF-5[26] and synthesized MOF@QDs/x CTAB (x = 0.1, 0.2, 0.3). (B) SEM image of MOF@QDs/0.3 CTAB sample.

The recorded diffractograms (**Figure 7A**) of the different MOF@QDs/x CTAB samples show no noticeable difference compared with samples synthesized without QDs. There is simply a slight shift of the diffraction peaks for the MOF@QDs/0.3 CTAB sample towards the low angles ($\Delta 2\theta = 2°$), which is currently not explained. SEM image (**Figure 7B**) reveal the same morphologies as those obtained without QDs. CTAB-caused MOF-5 porosity is still apparent. The incorporation of QDs into the MOF-5 structure does not appear to alter the latter.

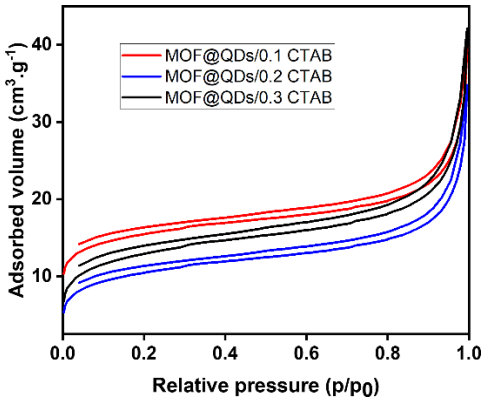

Figure 8. Adsorption and desorption isotherms of MOF@QDs/x CTAB (x = 0.1, 0.2, 0.3).

Then, nitrogen physisorption measurements were used to assess the evolution of the specific surface areas of samples after QD encapsulation (**Figure 8**). The isotherms still correspond to type I. However, specific surface area values decreased significantly after insertion of QDs (**Table 7**). These decreases may result from the insertion of QDs into the porosity of the materials, which completely obstruct the various pores. Measurement of the specific area allows us to conclude that the QDs are well-encapsulated within the MOF-5 crystals.

Table 7. Specific surface area (BET) and pore size (BJH) analyses on MOF-5/x CTAB samples.

x CTAB	S_{BET} before insertion ($m^2.g^{-1}$)	Pore size (BJH) (nm)	S_{BET} after insertion ($m^2.g^{-1}$)[a]
0.1	329	20	52
0.2	233	21	45
0.3	50	48	27

[a] insertion of 18 mg of QDs in each sample

Photoluminescence properties and PLQY were then measured on the various MOF@QDs/x CTAB samples obtained by the SIB approach. The maximum emission wavelength of all three samples is at 626 nm upon excitation at 375 nm (**Figure 9)**. However, for the sample prepared with the highest amount of CTAB (*i.e.*, 0.3 eq.), the emission intensity drops by ~20 %. This result is certainly linked to the loss of porosity, causing a greater extent of aggregation of the QDs, but further experiments are needed to better explain it.

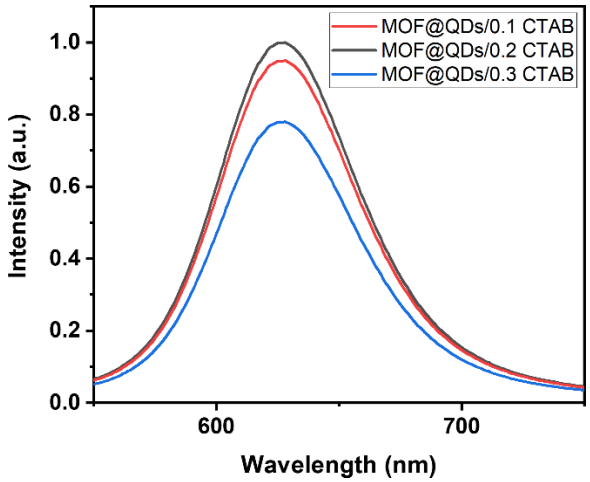

Figure 9. Emission spectra of MOF@QD/xCTAB samples (x = 0.1, 0.2, 0.3) recorded upon UV excitation (λ_{exc} = 375 nm).

Measurement of PLQY validates the hypotheses formulated by analysis of the emission spectra (**Figure S9**). Indeed, the quantity of QDs integrated seems similar in the three different samples, since the absorption coefficients of the different materials are comparable. The final material features high PLQY in the solid state, reaching 22% of $PLQY_{int}$ for the MOF@QDs/0.1 CTAB and MOF@QDs/0.2 CTAB samples, whereas this value falls to 15% for MOF@QDs/0.3 CTAB sample (**Table 8**). This decrease can be assigned to the well-known ACQ phenomenon between QDs InP/ZnS too close to each other within the structure.

Table 8. PLQY measured at 365 nm on the different MOF@QD/x CTAB samples prepared by the SIB method.

Sample	$PLQY_{int, 365nm}$ (%)	Absorption Coefficient	$PLQY_{ext, 365nm}$ (%)
MOF@QDs/0.1 CTAB	22	0.71	15.6
MOF@QDs/0.2 CTAB	22	0.82	18.0
MOF@QDs/0.3 CTAB	15	0.82	12.3

Unlike materials synthesized by the BAS method, the porosity is large enough to accommodate QDs. In principle, this would also imply the possibility of a release of these QDs over time in the presence of solvent. This effect was quantified by measuring the evolution of the emission of the MOF@QD/x CTAB samples after several hours in chloroform. 0.100 g of MOF@QD/0.3 CTAB powder were placed in 10 mL of chloroform for several hours. For each time point, the powder was centrifugally rewashed and dried, then the luminescence spectrum was recorded (**Figure S10**). As expected, the emission intensity of the MOF@QDs/0.3 CTAB sample decreases over time in the presence of chloroform. However, after 10 h a limit (22% loss) seems to have been reached

with luminescence virtually unchanged until 48 hours). This study confirms that the SIB approach results in the majority of QDs being quite firmly embedded in the MOF-5 structure.

CONCLUSION

In the present work, we have investigated and compared two distinct methods aiming to incorporate InP/ZnS quantum dots (QDs) into the MOF-5 structure and conducted a comparative analysis between them.

The *bottle around the ship* (BAS) method involving the synthesis the MOF-5 around the surface ligand exchanged InP/ZnS QDs. Despite the ease of MOF-5 (room temperature and mildly basic conditions), the ligand exchange process causes a drastic reduction of the QDs' PLQY. Thus, the resulting hybrid material exhibits red luminescence in the solid state with a maximum $PLQY_{ext}$ of 7.2 %.

On the other hand, the *ship in the bottle* (SIB) approach, consists in the insertion of the QDs through capillarity within a pre-synthesized MOF possessing greater porosity. We modified an existing synthesis protocol by incorporating CTAB, serving as a structuring agent. This enabled the isolation of mesoporous MOF-5 at room temperature in basic conditions. The incorporation of QDs into the MOF-5 structure is accomplished simply through solvent evaporation. The final material obtained demonstrates superior luminescence properties in the solid state, yielding a maximum $PLQY_{ext}$ of 18%, outperforming the materials prepared via the BAS method.

While the SIB technique appears more promising for achieving bright luminescence, it is important to note that the materials prepared using the BAS method exhibit no leaching over time in the presence of solvent. The BAS approach allows the creation of solid-state luminescent materials with more modest optical properties but larger specific surface areas, potentially advantageous in detection applications or when utilized with other types of QDs (*e.g.*, for

catalysis). Despite a certain leaching phenomenon observed in presence of solvent, the SIB approach facilitates the straightforward encapsulation of nanomaterials in matrices, while retaining luminescence properties in the solid state. This comparative study provides insights into the trade-offs between optical performance, stability, and surface area, offering avenues for tailored applications of cadmium-free MOF@QD hybrids.

ASSOCIATED CONTENT

Supporting Information. The following file is available free of charge.

Method for the determination of the concentration of InP QDs, Supplementary figures: x-ray diffraction, microscopy, spectroscopic characterizations, PLQY measurements, photographs of samples (PDF)

AUTHOR INFORMATION

Present Addresses

†Université de Lyon, ENS de Lyon, CNRS, Laboratoire de Chimie UMR 5182, F-69342 Lyon, France

Corresponding Authors

Federico. Cisnetti federico.cisnetti@uca.fr (https://orcid.org/0000-0002-9446-4601), Damien Boyer, damien.boyer@sigma-clermont.fr (https://orcid.org/0000-0003-2126-6468).

Author Contributions

The manuscript was written through contributions of all authors. All authors have given approval to the final version of the manuscript.

Funding Sources

A.T. and R. V. doctoral fellowships were funded by the French Ministry of Higher Education and Research for their doctoral fellowships

ACKNOWLEDGMENT

Franck Tessier is acknowledged for physisorption analyses. The CICS (Centre Imagerie Cellulaire Santé) is acknowledged for Microscopy.

REFERENCES

(1) Bruchez, M.; Moronne, M.; Gin, P.; Weiss, S.; Alivisatos, A. P. Semiconductor Nanocrystals as Fluorescent Biological Labels. *Science (1979)* **1998**, *281* (5385), 2013–2016.

(2) Geiregat, P.; Van Thourhout, D.; Hens, Z. A Bright Future for Colloidal Quantum Dot Lasers. *NPG Asia Mater.* **2019**, *11* (1), 41.

(3) Triana, M. A.; Hsiang, E.-L.; Zhang, C.; Dong, Y.; Wu, S.-T. Luminescent Nanomaterials for Energy-Efficient Display and Healthcare. *ACS Energy Lett.* **2022**, *7* (3), 1001–1020.

(4) Cao, F.; Wang, S.; Wang, F.; Wu, Q.; Zhao, D.; Yang, X. A Layer-by-Layer Growth Strategy for Large-Size InP/ZnSe/ZnS Core–Shell Quantum Dots Enabling High-Efficiency Light-Emitting Diodes. *Chem. Mater.* **2018**, *30* (21), 8002–8007.

(5) Farzin, M. A.; Abdoos, H. A Critical Review on Quantum Dots: From Synthesis toward Applications in Electrochemical Biosensors for Determination of Disease-Related Biomolecules. *Talanta* **2021**, *224*, 121828.

(6) Chen, B.; Li, D.; Wang, F. InP Quantum Dots: Synthesis and Lighting Applications. *Small* **2020**, *16* (32), 2002454.

(7) Reiss, P.; Carrière, M.; Linchenau, C.; Vaure L.; Tamang, S. Synthesis of Semiconductor Nanocrystals, Focusing on Nontoxic and Earth-Abundant Materials. *Chem. Rev.* **2016**, *116* (18), 10731–10819.

(8) Chung, H.; Cho, K.-S.; Koh, W.-K.; Kim, D.; Kim, J. Composition-Dependent Trap Distributions in CdSe and InP Quantum Dots Probed Using Photoluminescence Blinking Dynamics. *Nanoscale* **2016**, *8* (29), 14109–14116.

(9) Jasinski, J.; Leppert, V. J.; Lam, S.-T.; Gibson, G. A.; Nauka, K.; Yang, C. C.; Zhou, Z.-L. Rapid Oxidation of InP Nanoparticles in Air. *Solid State Commun.* **2007**, *141* (11), 624–627.

(10) Tessier, M. D.; Baquero, E. A.; Dupont, D.; Grigel, V.; Bladt, E.; Bals, S.; Coppel, Y.; Hens, Z.; Nayral, C.; Delpech, F. Interfacial Oxidation and Photoluminescence of InP-Based Core/Shell Quantum Dots. *Chem. Mater.* **2018**, *30* (19), 6877–6883.

(11) Li, C.; Hassan, A.; Palmai, M.; Snee, P.; Baveye, P. C.; Darnault, C. J. G. Colloidal Stability and Aggregation Kinetics of Nanocrystal CdSe/ZnS Quantum Dots in Aqueous Systems: Effects of Ionic Strength, Electrolyte Type, and Natural Organic Matter. *SN Appl. Sci.* **2022**, *4* (4), 101.

(12) Li, Y.; Wen, G.; Li, J.; Li, Q.; Zhang, H.; Tao, B.; Zhang, J. Synthesis and Shaping of Metal-Organic Frameworks: A Review. *Chem. Commun.* **2022**, *58* (82), 11488–11506.

(13) Wang, Q.; Astruc, D. State of the Art and Prospects in Metal-Organic Framework (MOF)-Based and MOF-Derived Nanocatalysis. *Chem. Rev.* **2020**, *120*, 1438–1511.

(14) Kreno, L. E.; Leong, K.; Farha, O. K.; Allendorf, M.; Van Duyne, R. P.; Hupp, J. T. Metal–Organic Framework Materials as Chemical Sensors. *Chem. Rev.* **2012**, *112* (2), 1105–1125.

(15) Li, H.; Wang, K.; Sun, Y.; Lollar, C. T.; Li, J.; Zhou, H. C. Recent Advances in Gas Storage and Separation Using Metal–Organic Frameworks. *Materials Today*. Elsevier B.V. March 1, 2018, pp 108–121.

(16) So, M. C.; Wiederrecht, G. P.; Mondloch, J. E.; Hupp, J. T.; Farha, O. K. Metal–Organic Framework Materials for Light-Harvesting and Energy Transfer. *Chem. Commun.* **2015**, *51* (17), 3501–3510.

(17) Aguilera-Sigalat, J.; Bradshaw, D. Synthesis and Applications of Metal-Organic Framework–Quantum Dot (QD@MOF) Composites. *Coord. Chem. Rev.* **2016**, *307*, 267–291.

(18) Wu, T.; Liu, X.; Liu, Y.; Cheng, M.; Liu, Z.; Zeng, G.; Shao, B.; Liang, Q.; Zhang, W.; He, Q. Application of QD-MOF Composites for Photocatalysis: Energy Production and Environmental Remediation. *Coord. Chem. Rev.* **2020**, *403*, 213097.

(19) Gutiérrez, M.; Zhang, Y.; Tan, J. C. Confinement of Luminescent Guests in Metal-Organic Frameworks: Understanding Pathways from Synthesis and Multimodal Characterization to Potential Applications of LG@MOF Systems. *Chem. Rev.* **2022**, *122* (11), 10438–10483.

(20) Ziegler, J.; Xu, S.; Kucur, E.; Meister, F.; Batentschuk, M.; Gindele, F.; Nann, T. Silica-Coated InP/ZnS Nanocrystals as Converter Material in White LEDs. *Adv. Mater.* **2008**, *20* (21), 4068–4073.

(21) Valleix, R.; Zhang, Q.; Boyer, D.; Boutinaud, P.; Chadeyron, G.; Feng, Y.; Okuno, H.; Réveret, F.; Hintze-Bruening, H.; Leroux, F. A First Wide-Open LDH Structure Hosting InP/ZnS QDs: A New Route Toward Efficient and Photostable Red-Emitting Phosphor. *Adv. Mater.* **2021**, *33* (38), 2103411.

(22) Stone, A. E. B. S.; Irgen-Gioro, S.; López-Arteaga, R.; Hupp, J. T.; Weiss, E. A. Encapsulating CdSe/CdS QDs in the MOF ZIF-8 Enhances Their Photoluminescence Quantum Yields in the Solid State. *Chem. Mater.* **2022**, *34* (4), 1921–1929.

(23) Kumagai, K.; Uematsu, T.; Torimoto, T.; Kuwabata, S. Photoluminescence Enhancement by Light Harvesting of Metal-Organic Frameworks Surrounding Semiconductor Quantum Dots. *Chem. Mater.* **2021**, *33* (5), 1607–1617.

(24) Zheng, H. Q.; Cui, Y.; Qian, G. Guest Encapsulation in Metal-Organic Frameworks for Photonics. *Acc. Mater. Res.* **2023**, *4* (11), 982–994.

(25) Karmakar, A.; Li, J. Luminescent MOFs (LMOFs): Recent Advancement towards a Greener WLED Technology. *Chem. Commun.* **2022**, *58* (77), 10768–10788.

(26) Eddaoudi, M.; Kim, J.; Rosi, N.; Vodak, D.; Wachter, J.; O'Keeffe, M.; Yaghi, O. M. Systematic Design of Pore Size and Functionality in Isoreticular MOFs and Their Application in Methane Storage. *Science (1979)* **2002**, *295* (5554), 469–472.

(27) Iswarya, N.; Kumar, M. G.; Rajan, K. S.; Balaguru, R. J. B. Synthesis, Characterization and Adsorption Capability of MOF-5. *Asian J. Sci. Res.* **2012**, *5* (4), 247–254.

(28) Chen, B.; Wang, X.; Zhang, Q.; Xi, X.; Cai, J.; Qi, H.; Shi, S.; Wang, J.; Yuan, D.; Fang, M. Synthesis and Characterization of the Interpenetrated MOF-5. *J. Mater. Chem.* **2010**, *20* (18), 3758–3767.

(29) Tranchemontagne, D. J.; Hunt, J. R.; Yaghi, O. M. Room Temperature Synthesis of Metal-Organic Frameworks: MOF-5, MOF-74, MOF-177, MOF-199, and IRMOF-0. *Tetrahedron* **2008**, *64* (36), 8553–8557.

(30) Tsao, C.-S.; Yu, M.-S.; Chung, T.-Y.; Wu, H.-C.; Wang, C.-Y.; Chang, K.-S.; Chen, H.-L. Characterization of Pore Structure in Metal−Organic Framework by Small-Angle X-Ray Scattering. *J. Am. Chem. Soc.* **2007**, *129* (51), 15997–16004.

(31) Habib, N. R.; Asedegbega-Nieto, E.; Taddesse, A. M.; Diaz, I. Non-Noble MNP@MOF Materials: Synthesis and Applications in Heterogeneous Catalysis. *Dalton Trans.* **2021**, *50* (30), 10340–10353.

(32) Ren, J.; Li, T.; Zhou, X.; Dong, X.; Shorokhov, A. V.; Semenov, M. B.; Krevchik, V. D.; Wang, Y. Encapsulating All-Inorganic Perovskite Quantum Dots into Mesoporous Metal Organic Frameworks with Significantly Enhanced Stability for Optoelectronic Applications. *J. Chem. Eng.* **2019**, *358*, 30–39.

(33) Chang, S.; Zhang, X.; Wang, Z.; Han, D.; Tang, J.; Bai, Z.; Zhong, H. Alcohol-Soluble Quantum Dots: Enhanced Solution Processability and Charge Injection for Electroluminescence Devices. *IEEE J. Sel. Top. Quantum Electron.* **2017**, *23* (5), 1900708.

(34) Hafizovic, J.; Bjørgen, M.; Olsbye, U.; Dietzel, P. D. C.; Bordiga, S.; Prestipino, C.; Lamberti, C.; Lillerud, K. P. The Inconsistency in Adsorption Properties and Powder XRD Data of MOF-5 Is Rationalized by Framework Interpenetration and the Presence of Organic and Inorganic Species in the Nanocavities. *J. Am. Chem. Soc.* **2007**, *129* (12), 3612–3620.